Collapse test and moment capacity of the Ruytenschildt reinforced concrete slab bridge

Lantsoght, Eva; van der Veen, Cor; de Boer, A; Hordijk, Dick

DOI
10.1080/15732479.2016.1244212

Publication date
2016

Document Version
Accepted author manuscript

Published in
Structure and Infrastructure Engineering

Collapse test and moment capacity of the Ruytenschildt Reinforced Concrete Slab Bridge

Eva Olivia Leontien Lantsoght (corresponding autor)

Concrete Structures, Delft University of Technology, Delft, The Netherlands

Stevinweg 1, 2628CN Delft, the Netherlands, Tel: +31152787449, E.O.L.Lantsoght@tudelft.nl

Politecnico, Universidad San Francisco de Quito, Quito, Ecuador

Diego de Robles y Pampite, Sector Cumbaya, EC 170157 Quito, Ecuador, Tel: +5932297-1700 ext. 1186, elantsoght@usfq.edu.ec

Cor van der Veen

Concrete Structures, Delft University of Technology, Delft, The Netherlands

Stevinweg 1, 2628CN Delft, the Netherlands, Tel: +31152784577, C.vanderveen@tudelft.nl

Ane de Boer

Rijkswaterstaat, Department of Infrastructure – Section Bridges and Viaducts, Ministry of Infrastructure and the Environment, the Netherlands

H12, P.O. Box 24057, 2502MB Utrecht, the Netherlands, Tel +31887972083, ane.de.boer@rws.nl

Dick Hordijk

Concrete Structures, Delft University of Technology, Delft, The Netherlands

Stevinweg 1, 2628CN Delft, the Netherlands, Tel: +31152784434, D.A.Hordijk@tudelft.nl

Acknowledgement

This work was supported by the Province of Friesland and the Dutch Ministry of Infrastructure and the Environment (Rijkswaterstaat).

Collapse test and moment capacity of the Ruytenschildt Reinforced Concrete Slab Bridge

A large number of existing reinforced concrete solid slab bridges in the Netherlands are found to be insufficient for shear upon assessment. However, research has shown additional sources of capacity in slab bridges, increasing their total capacity and possibly changing their failure mode. Previous testing was limited to half-scale slab specimens cast in the laboratory. To study the full structural behavior of slab bridges, testing to failure of a bridge is necessary. Research on load testing is carried out in order to develop load testing guidelines. In August 2014, a bridge was tested in two spans. The bridge was load tested, and additional cycles until yielding occurred in the reinforcement were added to the experiment. Though calculations with current design provisions showed that the bridge could fail in shear, the field test showed failure in flexure before shear. The unity check for flexure was determined. The experiment shows that the methods for rating of existing reinforced concrete slab bridges are conservative.

Keywords: assessment; bridge tests; concrete slabs; field tests; flexural strength; shear strength

1. Introduction

The major expansion of the Dutch road network occurred during the decades of reconstruction after the Second World War. Therefore, the majority of the existing bridges in the Netherlands date from prior to 1976. These bridges were designed for the live loads of that era, which are considerably lower than the current design live loads from the Eurocode NEN-EN 1991-2:2003 (CEN, 2003). At the same time, the shear capacity calculated according to the currently governing Eurocode 2 NEN-EN 1992-1-1:2005 (CEN, 2005) is lower than according to the previously used Dutch codes, such as the VBC 1977 (Stichting Commissie Voorschriften Beton, 1977). These code changes resulted in a large number of existing Dutch reinforced concrete bridges to be found insufficient for shear (Eva O.L. Lantsoght, van der Veen, de Boer, & Walraven,

2013). In total, about 600 reinforced concrete slab bridges are subject of discussion.

Over the past years, research at Delft University of Technology studied the behaviour and shear capacity of reinforced concrete slab bridges. Shear tests on slab specimens under concentrated loads close to supports (E.O.L. Lantsoght, van der Veen, De Boer, & Walraven, 2014; Eva O.L. Lantsoght, van der Veen, & Walraven, 2013) resulted in the conclusions that the capacity of slabs under concentrated loads benefits significantly from the transverse load distribution capacity of slabs (Eva O.L. Lantsoght, van der Veen, de Boer, & Walraven, in press). These experiments led to recommendations with regard to the effective width in shear (E.O.L. Lantsoght, De Boer, Van der Veen, & Walraven, in press) and the distribution of the peak stresses in linear finite element models (E.O.L. Lantsoght, De Boer, & van der Veen, 2014; Eva O.L. Lantsoght, de Boer, Van der Veen, & Walraven, 2013). A procedure for finding the capacity of cracked cross-sections of slab bridges was also developed (Eva O. L. Lantsoght, van der Veen, Walraven, & de Boer, 2016).

The past few years, Delft University of Technology also executed a number of load tests on slab bridges. Load tests can be interesting when the effect of material deterioration is unknown (such as for viaducts with alkali-silica reaction, or corrosion effects (Pape and Melchers, 2010)), when the structural system raises concerns (e.g. when it is unknown how much movement can take place in bearings and joints reaching the end of their service life), or when insufficient information is available about the structure to carry out an assessment. The aim of the load tests executed by Delft University of Technology is to develop a guideline for proof loading of structures. This guideline (R. Koekkoek, Lantsoght, Yang, De Boer, & Hordijk, 2016) should encompass the methods for determining the proof load (based on a certain reliability

level) and the stop criteria (criteria based on the field measurements that indicate when the experiment needs to be prematurely aborted because the structure signals distress).

In 2014, the opportunity arose to test the Ruytenschildt Bridge, owned by the province of Friesland and scheduled for demolition. Since the bridge needed replacement, it was possible to carry out a load test, and to load the bridge until failure. The focus of this paper will be the ultimate capacity and the flexural analysis of the Ruytenschildt Bridge. Since there are doubts about the shear capacity of existing reinforced concrete slab bridges, the critical loading position that was used in the experiments on the Ruytenschildt Bridge was the critical position for a shear failure. Extra attention was paid to a possible failure in shear, since a shear failure is a brittle failure mode, which could result in a collapse of a structure without much warning behaviour of the structure.

2. Literature review

2.1. Load testing of bridges

Two distinct types of load tests exist, each with their different purpose. Diagnostic load tests (Farhey, 2005; Jauregui, Licon-Lozano, & Kulkarni, 2010; Moses, Lebet, & Bez, 1994; Olaszek, Lagoda, & Ramon Casas, 2014; Russo, Wipf, & Klaiber, 2000) use a low load and verify if the stiffness and behaviour of the bridge is as expected. Several countries, such as Italy (Veneziano, Galeota, & Giammatteo, 1984), Switzerland (Bruehwiler, Vogel, Lang, & Luechinger, 2012) and France (Cochet et al., 2004b) require a diagnostic load test upon opening of a bridge. Proof load tests (Cai & Shahawy, 2003; Casas & Gómez, 2013; Moses et al., 1994; Saraf, Sokolik, & Nowak, 1996) use a higher load and proof a certain capacity of a bridge. Ideally, this capacity can be linked to a probability of failure of the bridge, so that the result of the test and

analysis is an estimate of the safety. Guidelines for carrying out load tests and when a test needs to be stopped because the structure indicates damage (the so-called “stop criteria”) are available in Germany (Deutscher Ausschuss für Stahlbeton, 2000) for the limit state of flexure. In the United States, a relatively old manual exists that links load tests to bridge rating (NCHRP, 1998) as well as a guideline for load testing of buildings (ACI Committee 437, 2013), which includes stop criteria for the limit state of flexure. Other available guidelines are from the United Kingdom (The Institution of Civil Engineers - National Steering Committee for the Load Testing of Bridges, 1998), from Ireland (NRA, 2014) and from France (Cochet et al., 2004a).

The stop criteria are necessary to identify the maximum load for a non-destructive field test. Loading beyond this point will cause irreversible damage. The first symptoms of damage in concrete bridges for flexure are identified based on strains in the concrete and reinforcement steel, as described by the German guideline (Deutscher Ausschuss für Stahlbeton, 2000). Moreover, to avoid damage in the tested bridge, cycles of loading are used. After every cycle, the residual deformation is studied. Both the German guideline and ACI 437-2M.13 study residual deformations to analyse if further loading is safe. When acoustic emission sensors are used, these measurements can also be used to study the formation and growth of cracks in the bridge (Anay et al., 2016; Olaszek et al., 2012; Yang and Hordijk, 2015). So far, it is possible to capture the first signs of damage for the limit state of flexure, and to stop loading with a safe margin prior to the formation of irreversible damage. For the limit state of shear, which is a brittle failure mode, stop criteria still need to be developed, and currently research on this topic is being carried out (Schacht, Bolle, Curbach, & Marx, 2016).

In the Netherlands, Delft University of Technology is developing a guideline for proof loading of structures. The goal of the guideline is to consider the limit states of shear and flexure, and to define stop-criteria for these limit states that are suitable for both new and existing structures. The following viaducts have been proof loaded under heavy instrumentation for the development of the guideline: the viaduct Vlijmen-Oost (S. Fennis, van Hemert, Hordijk, & de Boer, 2014), the Halvemaans Bridge (S. A. A. M. Fennis & Hordijk, 2014) in Alkmaar, the viaduct Zijlweg (R.T. Koekkoek, Lantsoght, & Hordijk, 2015) and the viaduct De Beek (R.T. Koekkoek, Lantsoght, Yang, & Hordijk, 2016). The Ruytenschildt Bridge is the only bridge so far in this program of bridge tests that has been tested to failure.

2.2. Previous experiments to failure

A limited number of bridge tests to failure is available in the literature, see Table 1. The majority of the tested bridges were slab bridges and flexural failure was the dominating failure mode. Another test to failure from the literature is the testing of the Thurloxton underpass (Cullington, Daly, & Hill, 1996). This test is not included in the table, because saw cuts over 1 m width were used, preventing the slab from developing transverse load redistribution. Similarly, for the case of the Maumee River Bridge, a prestressed box beam from the structure was dismantled and tested isolated from the original structure (Allbright et al. 1995). For similar reasons, the tests of Halsey and Miller (1996) and Rogers et al. (2012) are not included in Table 1. The model bridge tested in the laboratory by Roschke and Pruski (2000) might be of interest to the readers, but is not included in Table 1 because this experiment deals with a scale model of a posttensioned slab bridge. Before testing the Reibersdorf Overpass Bridge (Siringoringo et al. 2013), damage was introduced by cutting one of the piers at the

footing level, changing the structural behaviour, and therefore this test is not included in Table 1.

3. Description of bridge

3.1. Location and history

The Ruytenschildt Bridge, see Figure 1, is located in the national road N924, which connects the villages of Lemmer and Heerenveen in the province of Friesland (The Netherlands). The bridge is situated over a waterway connecting the Tjeuker Lake to the Vierhuister Canal. The year of construction of the bridge is 1962. In 2014, the bridge was demolished and rebuilt at a larger clearance, so that taller boats can pass the underlying waterway. The bridge carries two lanes (one lane in each direction) as well as a single bike lane.

3.2. Geometry

The superstructure of the Ruytenschildt Bridge was a continuous reinforced concrete solid slab bridge of five spans. At the supports, cross-beams were cast integrally onto the piers. The bridge had a skew angle of 18^{o}. Drawings of the cross-section, top view and side view are given in Figure 2. In Figure 2a, the stages of demolition are indicated on the cross-section. As at least one motor lane and one bicycle lane were needed throughout the replacement of the bridge, the contractor and owner opted for a staged demolition process. The hatched part of the cross-section in Figure 2a was isolated from the rest of the structure with a saw cut. The width of this part was 7.37 m. The remaining part of the bridge was used to carry one lane of traffic. The bike traffic was deviated over a floating pontoon. While the traffic used one lane, the Ruytenschildt Bridge was tested in spans 1 and 2 (see Figure 2c). As can be seen in Figure 2b, the thickness of the bridge deck slab was 550 mm.

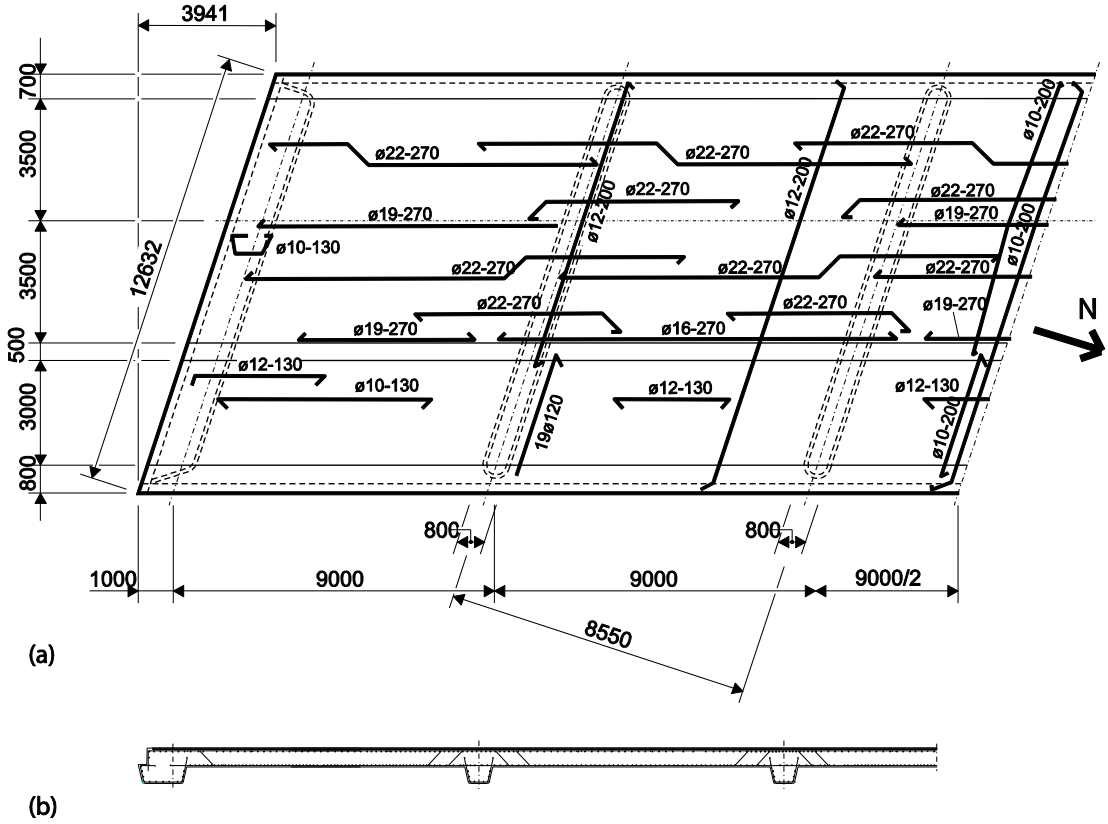

Figure 3 shows a plan view and cross-section of the reinforcement layout. An overview of the available reinforcement is given in Table 2. In span 1, 2 layers of φ = 22 mm with a spacing of 270 mm and 1 layer of ϕ = 19 mm with a spacing of 270 mm is available, so that A_s = 3866 mm^2/m in span 1. In span 2, 2 layers of ϕ = 22 mm with a spacing of 270 mm and 1 layer of ϕ = 16 mm with a spacing of 270 mm is available, so that A_s = 3650 mm^2/m in span 1. Over support 2, 4 layers of ϕ = 22 mm with a spacing of 270 mm are available, so that A_s = 5632 mm^2/m over support 2. The mentioned layers are in the width direction, reducing the spacing between the bars but not changing the effective depth of the cross-section.

3.3. Material Properties

The concrete compressive strength was derived based on the results of 62 cores. The average cube compressive strength, recalculated from the core samples, was f_{cm} = 40

MPa with a characteristic value of f_{ck} = 25 MPa (E.O.L. Lantsoght, 2015). Further analysis of the cores, however, indicated that the surface treatment needed improvement. Currently, a level cut or epoxy glue can be used to create a level surface for the test. Experiments showed that even with a level cut, the surface tends not to have the correct properties. In the lab, a calibration factor was derived to correct for this discrepancy by comparing the compressive strength of cores with a level cut to the compressive strength of cores with an epoxy glue to create an even surface for testing. The cores with the surface treatment with epoxy glue were taken from the beams that were sawn out of the bridge and taken to the laboratory for additional testing. The corrected value of the average cube compressive strength was f_{cm} = 63 MPa (Yang 2015), which converts to a cylinder compressive strength $f_{cm,cyl}$ = 52 MPa. The asphalt layer was present on the cores and was measured as 51 mm on average.

The type of reinforcement steel in the Ruytenschildt Bridge was the old Dutch type QR 24. This reinforcement steel has a characteristic yield strength f_{yk} of 240 MPa. Tests on samples taken from the bridge resulted in a yield strength f_y = 352 MPa and an ultimate strength f_u = 435 MPa for the ϕ 12 mm bars and f_y = 309 MPa and f_u = 360 MPa for the ϕ 22 mm bars.

4. Prediction of capacity

4.1. Shear capacity

Average material parameters and expressions for the average cross-sectional capacity are used to estimate the capacity in the bridge test. For this analysis, the shear capacity is calculated according to NEN-EN 1992-1-1:2005 (CEN, 2005). For members without shear reinforcement and without prestressing, the average shear capacity can be determined as (with f_{cm} in [MPa] and d_l in [mm]):

$$V_{R,c} = C_{R,c} k \left(100 \rho_l f_{cm}\right)^{1/3} b_w d_l \geq v_{min} b_w d_l$$

$$k = 1 + \sqrt{\frac{200}{d_l}} \leq 2.0$$

According to the Eurocode procedures, the value of v_{min} may be chosen nationally, and is recommended as (for average values, with f_{cm} in [MPa]):

$$v_{min} = 0.035 k^{3/2} f_{cm}^{1/2} \text{ in [MPa]}$$

To calibrate the formula for finding average values, a statistical analysis (König and Fischer 1995) showed that a factor of 0.15 can be used (Lantsoght, 2013). The effective width in shear for slabs (E.O.L. Lantsoght, de Boer, van der Veen, & Walraven, 2015) is determined based on a 45^o load spreading from the far side of the axle to the face of the support for straight slabs. However, for skewed slabs, different interpretations of this recommendation are possible: b_{str}, the effective width for a straight slab, b_{skew} with horizontal load spreading under 45^o from the far side of the wheel print to the face of the support, and b_{para} based on a load spreading parallel to the straight case. Figure 4 shows these different options, as well as the critical position for shear at 2.5d_l (Eva O.L. Lantsoght, van der Veen, de Boer, et al., 2013; Rijkswaterstaat, 2013b). For both spans, the face-to-face distance between the first axle of the load testing tandem and the support was taken as 2.5d_l. This position is considered the critical loading position for shear in straight slabs, and was identified as such based on experiments on slabs under concentrated loads failing in shear (Lantsoght et al. 2013b).

Different interpretations for the capacity of skewed slab bridges are possible as there is no consensus yet on how to determine the effect of the skew. In the Netherlands, for the assessment of skewed slab bridges, a set of skew factors is used that increase the load effects (Rijkswaterstaat, 2013a) depending on the skew angle of the bridge. These factors have been determined based on a parameter study with linear

finite element models. A similar approach, but leading to different factors, is available from Canada (Theoret, Massicotte, & Conciatori, 2012) and similar studies have been carried out in the United States (Menassa, Mabsout, Tarhini, & Frederick, 2007). The number of experiments available in the literature is very limited (R. J. Cope & Rao, 1983; R.J. Cope, Rao, & Edwards, 1983; Cusens, 1987), and a first conclusion of these experiments is that the failure mode changes as the skew angle increases and the position of the wheel prints is kept unchanged. Until more experimental results are available, no definite answers can be given on the effect of the skew angle on the shear capacity of reinforced concrete slab bridges.

The results of the calculations are presented in Table 2 based on the maximum total tandem load, P_{tot}, at which shear failure is expected in the bridge test. Transverse load redistribution in slabs subjected to loads close to supports increases the shear strength in straight slabs by 1.466 (Eva O.L. Lantsoght, 2012) as a characteristic value when compared to the Eurocode prediction. This factor was derived from a series of experiment on slabs in shear in which the majority of the parameters that influence the shear capacity, except the specimen height, were varied. The slabs that were used in these experiments had a height of 300 mm, and an effective depth d_l of 265 mm. $P_{tot,slab}$ takes this multiplication factor into account. However, in skewed slabs, stress concentrations in the obtuse corner have a negative effect on the shear capacity (R.J. Cope et al., 1983). P_{tot} and $P_{tot,slab}$ are thus the bounds between which the shear capacity is expected to lie. The value of the maximum load P_{tot} for which shear failure is expected, is determined in the Quick Scan sheet (Vergoossen, Naaktgeboren, ‘t Hart, De Boer, & Van Vugt, 2013).

4.2. Flexural capacity

The flexural capacity is subdivided into the moment at cracking $M_{cr,}$ yielding M_y and the

ultimate M_u, based on a traditional beam analysis and the present reinforcement. The cracking moment M_{cr} is determined as:

$$M_{cr} = \frac{f_r y_{tension}}{I_{gross}} \text{ with } f_r = \frac{7.5}{12}\sqrt{f_{cm}} \text{ with } f_{cm} \text{ in [MPa]}$$

The moment capacity at yielding, M_y, is based on Thorenfeldt's stress-strain diagram for concrete. The stress-strain diagram of Thorenfeldt for f_{cm} = 52 MPa is shown in Figure 5. A linear strain diagram over the depth of the cross-section is assumed, with ε_c the strain in the extreme compression fiber:

$$M_y = C_c\left(d_l - k_2 c_y\right) + C_s\left(d_l - d'\right)$$

$$k_2 = 1 - \frac{2\left(\frac{\varepsilon_c}{\varepsilon_0} - \arctan\left(\frac{\varepsilon_c}{\varepsilon_0}\right)\right)}{\left(\frac{\varepsilon_c}{\varepsilon_0}\right)^2 \times \beta_1}$$

$$\varepsilon_0 = \frac{f_{cm}}{E_c}\left(\frac{n_{th}}{n_{th}-1}\right)$$

$$n_{th} = 0.8 + \frac{f_{cm}}{17.24MPa}$$

$$\beta_1 = \frac{\ln\left(1 + \left(\frac{\varepsilon_c}{\varepsilon_0}\right)^2\right)}{\frac{\varepsilon_c}{\varepsilon_0}}$$

$$C_c = \beta_1 f_{c,th} \times b \times c_y$$

$$f_{c,th} = \frac{0.9 f_{cm} \times n_{th} \times \frac{\varepsilon_c}{\varepsilon_0}}{n_{th} - 1 + \frac{\varepsilon_c}{\varepsilon_0}^{n_{th} k_{th}}}$$

$$k_{th} = \begin{cases} 1 \text{ if } \frac{\varepsilon_c}{\varepsilon_0} \le 1 \\ 0.67 + \frac{f_{cm}}{62.07MPa} \text{ if } \frac{\varepsilon_c}{\varepsilon_0} > 1 \end{cases}$$

$$k_{th} = 0.67 + \frac{f_{cm}}{62.07MPa}$$

The ultimate moment capacity, M_u, is based on a rectangular stress block diagram and can be determined as:

$$M_u = 0.85 f_{cm} \beta_{ult} c_{ult} b \left(d_l - \frac{\beta_{ult} c_{ult}}{2} \right) + A_{s,comp} f_s' \left(d_l - d' \right)$$

$$\beta_{ult} = \begin{cases} 0.85 \text{ if } f_{cm} \leq 28\text{MPa} \\ 0.85 - 0.05 \dfrac{f_{cm} - 28\text{MPa}}{7\text{MPa}} \text{ if } 28 \text{ MPa} \leq f_{cm} \leq 55\text{MPa} \\ 0.65 \text{ if } f_{cm} \geq 55\text{MPa} \end{cases}$$

Table 2 contains the results of this analysis. These results are for the position of the load test, which is the critical position for shear. The critical position for shear was selected to investigate if there is a possibility for shear failure in existing reinforced concrete slab bridges. The corresponding maximum loads P_{cr}, P_y and P_u are based on a model of a five-span beam.

5. Testing of the bridge

5.1. Test setup

The load used in the test on the Ruytenschildt Bridge had the geometry of the design tandem from live load model 1 from NEN-EN 1991-2:2003 (CEN, 2003): four wheel prints of 400 mm square with a transverse distance of 2 m and a longitudinal distance of 1.2 m. As the goal of the experiment was, amongst others, to verify if shear failure is possible (which is a brittle failure mode that could cause an unexpected collapse of a bridge with insufficient capacity), the face-to-face distance between the axle and the cross-beam at the support was 2.5d_l, the critical position for shear (Eva O.L. Lantsoght, van der Veen, de Boer, et al., 2013; Rijkswaterstaat, 2013c). In the transverse direction, the critical position is in the obtuse corner (R. J. Cope, 1985) and as close to the edge as possible, which is the situation that creates the largest shear stress concentrations. The

edge distance was 800 mm in span 1 and 600 mm in span 2. The edge distance was taken as small as possible.

One danger in testing a bridge to failure is the possibility that the entire loading setup falls down when the bridge collapses. To avoid this possibility, the bridge was gradually loaded through a load spreader construction as shown in Figure 6: ballast blocks were placed on the load spreader over the support, and then hydraulic jacks gradually applied the load onto the slab at the loading position during the experiment. Unloading at the jacks would result when large deformations at failure occur.

5.2. Instrumentation

The instrumentation on the Ruytenschildt Bridge was elaborate, and served the purpose to study both proof loading and testing to failure. The measurements followed the deformations in the longitudinal and transverse direction with linear variable differential transformers (LVDTs) and laser triangulation sensors, the strain on the bottom surface with LVDTs on steel bars of 1 m, the crack width with LVDTs and the activity in the cracks with acoustic emission measurements. The full plan of instrumentation, with the measurement range of the sensors, is shown in Figure 7, which also includes the position of the wheel prints during the experiments in span 1 and span 2. In this drawing, AE denotes the positions of the acoustic emissions sensors. The positions of LVDTs 7 through 10 were determined in the field, where the largest existing cracks were selected for monitoring during the test. The acoustic emission sensors were used for research purposes, as the possibility is explored to use acoustic emission measurements as a stop criterion, especially for a brittle failure mode like shear. This topic is currently under research.

6. Results

6.1. Span 1

The loading scheme and the measurements of the laser covering the maximum displacement for both spans is shown in Figure 8. For the acoustic emissions measurements and to check for nonlinear behaviour, typically three cycles were carried out to each load level. The values of the maximum loads in the field test are given in Table 3 for comparison.

On span 1, failure did not take place. The maximum available load provided by the ordered ballast blocks was 3049 kN. Flexural distress was observed, but flexural failure did not take place.

The calculated shear capacity was higher than the maximum load that was applied and shear distress was not observed. The maximum flexural capacity as calculated with the average material parameters was also higher. The Ruytenschildt Bridge is an integral bridge, which leads to a support moment over the end support. In practice, the rotational stiffness of the support is difficult to estimate, and the support was conservatively modelled as a hinge. As a result of the end moment, the span moment that occurs under a given loading will be smaller than calculated when assuming a hinged support.

6.2. Span 2

Since failure in span 1 could not be achieved, more counterweights were ordered for the next test on span 2. The deck was tested at its critical position for shear. For this test, the maximum load was 3991 kN, and flexural failure of the slab occurred. Moreover, the pier of support 2 underwent a settlement of 15 mm right after the application of the maximum load. The loading scheme and the displacement versus time are shown in Figure 8. In Figure 9, the load-displacement diagram is shown. It can be seen that non-

linear behaviour starts to occur around 2050 kN. As a result of delayed recovery, the final residual settlement at the pier was 8 mm. The maximum applied load was smaller than the load necessary to achieve a shear failure according to most calculation methods from Table 2. The resulting moment was somewhere between the yielding and ultimate moment of the slab as calculated in Table 2, which corresponds to the observations in the experiment. Yielding of the steel caused large cracks and deformations, but the load was not applied until the point of actually causing collapse of the entire deck and breaking of the steel reinforcement or crushing of the concrete compression zone. An estimate of the shear capacity cannot be provided because there was no indication of shear distress or of shear failure.

As failure was reached in the second span, the results and the measurements could be used to determine when the stop criteria from the German guideline and ACI 437.2M-13 were exceeded, and how far from or close to the failure load the load was when the stop criterion was exceeded (Tersteeg, 2015). Using the German guideline, a proof load test would be stopped at 2050 kN, when nonlinear behaviour was observed in the load-displacement diagram. The stop criterion for residual deflection was only exceeded at 3181 kN. Using ACI 437.2M-13, the stop criterion of the permanency ratio, based on ratios of maximum and permanent deflections, is exceeded at 3191 kN, the residual deflection at 3696 kN and the deviation from linearity index (based on the tangent of the load-displacement diagram) at 3700 kN. The test would have been stopped at 2050 kN, when nonlinear behaviour was observed in the load-displacement diagram. These observations confirm that for flexure, the stop criteria, and especially the use of instrumentation to follow the load-displacement diagram in real-time during the test, have indicated that the test needs to be stopped before reaching the failure load.

7. Analysis of bending moment capacity of Ruytenschildt Bridge

7.1. Description of finite element model and applied loads

To further analyse the moment capacity of the two tested spans of the Ruytenschildt Bridge, the Unity Checks for bending moment will be determined in more detail. The first step of the analysis is to construct a linear finite element model of the bridge. A linear finite element model of the slab with a width of 7.37 m and five spans of each 9 m was made in SCIA Engineer (Nemetschek Scia, 2016). The skew angle of 18^{o} of the bridge is modelled. All supports are modelled as hinges, neglecting the restraint at the end supports caused by the bridge being an integral bridge.

In this model, first the Eurocode loading is applied. The applied loading is the self-weight, the layer of asphalt of 51 mm and with a weight of 23 kN/m^3, and the live load from Load Model 1 from NEN-EN 1991-2:2003 (CEN, 2003). The distributed load of the live load model is 9 kN/m^2 in the first lane and 2.5 kN/m^2 in the second lane. Since the saw cut reduced the number of lanes to less than 3, the α_{qi} factors for determining the distributed lane load for bridges with multiple lanes from Load Model 1 are taken as 1. Two lanes fit the geometry, so that two design tandems are applied. The tandem in the first lane is 300 kN per axle and in the second lane 200 kN. The wheel print is 400 mm × 400 mm, with a transverse distance of 2 m and a distance between axles of 1.2 m. With this model, the most unfavourable position of the design tandems is sought. For flexure, the most unfavourable position results in the largest moment. The load combinations are determined by NEN 8700:2011 (Code Committee 351001, 2011). The analysis is carried out at the safety level "Reconstruction", which corresponds with a reliability index β = 3.3 and a reference period of 30 years (R. T. Koekkoek, Yang, Fennis, & Hordijk, 2015). The load factor on the self-weight and permanent loads is 1.15 and on the live loads 1.3. For the first and second span, the positions of the design

tandem for which the largest moments are found, as well as these moments, are given in Table 4.

In a next step, the proof load is applied to the finite element model. For this case, the distributed lane load and the permanent load of the asphalt, which was removed before the test, are omitted. The position is as used in the experiment; closer to the support to study a possible shear failure. The *x*-coordinate in the finite element model of the tandem was 3.39 m for the first span as a result of the skew. A total proof load of 3049 kN or of 762.25 kN per wheel print was applied for the first span. For the second span, a total proof load of 3991 kN or of 997.75 kN per wheel print was applied. The resulting moments for these positions and loads are given in Table 4. Figure 10 shows the moments m_x caused by the proof load tandem in span 1.

7.2. Plastic analysis

A plastic analysis of the first span was carried out with a beam model in MASTAN2 (Ziemian & McGuire, 2015). The load on the axles is increased until the yield moment is achieved in the span, after which a hinge is inserted where the yield moment is reached. Then, the method aims at increasing the load further until the yield moment (hogging moment) of the cross-section at continuous support is achieved. If plastic redistribution cannot take place, a moment larger than the yield moment occurs over the support, which means the development of a mechanism and collapse.

An axle load of 1184 kN is necessary to reach the yield moment in the span of 3925 kNm at the location of the second axle. Note that the same load was applied on both axles, so that the total load of the tandem is the double of the presented axle loads. If a hinge is then inserted at the location of the second axle, the moment over the continuous support becomes 13780 kNm. M_y at the support equals 5662 kNm, see Table

3, and no redistribution after the development of the plastic hinge can take place. A mechanism forms instead of a stable configuration. The maximum axle load in the test was 1524.5 kN. This analysis shows that the axle load to obtain yielding was 1184 kN. However, the effect of the integral bridge and the moment at the end support were not taken into account for this analysis, because there is no estimate of the restraint at the end support. Estimating the effect of the restrain would have been possible if span 1 would have been tested to failure, so that the restraint could have been derived from the observed moment diagram in the test.

In span 2, M_y was 3717 kNm, see Table 3, which corresponds to an axle load of 1766 kN. If a hinge is inserted at the second axle, the moment over the continuous support become 8013 kNm, which is larger than the capacity of 5662 kNm. A mechanism develops, as happened in the first span, and no further redistribution is possible after achieving yield at the location of the second axle. The maximum axle load in the test was 1995.5 kN. The calculated axle load to achieve yield was 1766 kN based on a beam model.

Based on the observed cracking, a more refined analysis can be carried out for the second span. In this refined analysis, the beam model is replaced by a slab model. An overview of the major cracks is shown in Figure 11. Table 5 then summarizes the resulting yielding moments for the present reinforcement, where the plastic moment $M_{plastic}$ is determined as the product of the length of the crack and the yield moment of the present reinforcement. Indications for yielding were observed in the experiment based on the nonlinearity of the load-displacement curve at a total load of 2050 kN on the tandem. This load corresponds with two axles of 1025 kN or a wheel load (four wheels) of 512.5 kN.

The SCIA Engineer (Nemetschek Scia, 2016) model, presented in the previous paragraph, is used for this refined analysis and a cut along crack 1 from Table 5 is made, see Figure 12. In a next step, the percentage of the load carried by 3.47 m (the crack length) is determined. The length of the crack is considered the length of the plastic hinge, as the observed cracking is an indication of the occurrence of yielding during the experiment. The percentage of load carried over the cracked distance of 3.47 m is determined based on the moment diagram along the cut. The analysis shows that 77.4% of the moment is carried by the part of the crack and that 22.6% is carried by the part of the section that is still linear elastic. The plastic hinge develops over a length of 3.47 m, so that 3.90 m remains linear elastic. In other words, the uncracked part of the width of the slab is considered to still be linear elastic at a total tandem load of 2050 kN. The total moment, integrated over the full width of the slab, in the cross-section caused by the wheel loads of 512.5 kN is 2271 kNm. The linear elastic part of the moment is calculated as:

$$LEpart = \frac{3.90\ \text{m}}{3.47\ \text{m}} \times 77.4\% \times 2271\ \text{kNm} = 1973\ \text{kNm}$$

In this linear elastic part, the moment can increase until reaching the yield moment of the cross-section, determined previously, so that:

$$LEpart_{\max} = \frac{3.90\ \text{m}}{3.47\ \text{m}} \times 77.4\% \times \xi = 2271\ \text{kNm}$$

The moment that can be achieved to reach yielding over the full width, including the linear elastic part, is ξ = 2614 kNm. This moment corresponds to an axle load of 1188 kN or a total load of 2376 kN based on a beam model in MASTAN2. This maximum value of the total load will be used to determine the Unity Check for bending moment.

7.3. Required proof load to reach maximum moment Eurocode loading

In this paragraph, it will be explained which value of the load applied on the tandem would result in the same maximum sectional moment as Eurocode live load model 1. In the first span, the maximum sagging moment for span 1 was found when the design tandems of the Eurocode live load model 1 were placed at 4.63 m from the support. In this part of the analysis, the proof load tandem (replacing live load model 1 from the Eurocode) is applied in the finite element model at this position (4.63 m), and the distributed lane load (which is part of live load model 1) and the asphalt layer, which was removed prior to the test, are removed to represent the testing conditions. The maximum load on the proof tandem to achieve the same highest moment as with the Eurocode loading is now sought. Note that the tandem for this analysis is placed farther into the span than what was used during the test. To achieve a design moment m_{ux}^{+} = 438.49 kNm/m, a total load on the proof load tandem of 1240 kN needs to be applied. This load is considerably lower than the maximum load that was achieved in the experiment of 3049 kN.

In the second span, the *x*-coordinate of the position was 14.50 m, or 5.50 m from support 2. To achieve the design moment m_{ux}^{+} = 330.44 kNm/m which results from applying the Eurocode loading (live load model 1), a total load on the proof load tandem of 1088 kN needs to be applied. This value is again significantly lower than the maximum load that was achieved in the experiment of 3991 kN.

To proof sufficient capacity in a proof load test for the safety level of "Reconstruction", the maximum value to be applied on the proof load tandem would be 1088 kN, and then the loading would be stopped. In this experiment, the load was increased beyond this value, because the Ruytenschildt Bridge was tested until failure.

7.4. Unity Checks

With the previous calculations, the Unity Check for bending moment is determined. The Unity Check for bending moment is the moment caused by the applied loading divided by the bending moment capacity of the cross-section. If the Unity Check value is lower than or equal to unity, sufficient capacity has been proven for the considered cross-section. The moment caused by the applied loading can be determined in two ways:

1. The moment caused by the proof load at a distance of $2.5d_l$ from the support.
2. The moment caused by the Eurocode loading (live load model 1) at the position that causes the largest bending moment (4.63 m from support 1 and 5.50 from support 2, for both spans respectively).

The capacity can also be determined in two ways:

1. From the bending moment capacity from Table 2.
2. From the refinement based on the formation of the plastic hinge over a part of the width of the slab. This method is only possible for span 2, where the measured cracks led to the refinement.

The values of the capacity side and the loading side are given here as the total load on the proof load tandem, so that the refinement based on the plastic redistribution after the formation of the crack in span 2 can be taken into account. An overview of the calculated loads and resulting Unity Checks is given in Table 6. The results indicated with “Unity Check” are based on the load corresponding to the maximum moment caused by the Eurocode loading, divided by the minimum capacity from the considered span given in Table 6. The result indicated with “Unity Check with proof load” are based on the applied load in the test. The calculated Unity Checks in Table 6 show that the bridge would rate sufficient for bending moment capacity in an assessment (UC < 1), and that during the experiment a significant larger capacity is found (UC > 1) as a

result of transverse redistribution and, for span 2, plastic redistribution. The methods for rating bridges are thus conservative.

The reader should keep in mind that the bridge was tested to failure at the critical position for shear. Regardless of this position, flexural failure was governing over shear failure for span 2, in which failure was achieved. When the moment caused by the proof load is used for the Unity Check, then it needs to be considered that the load to reach a flexural failure is higher than the load necessary to achieve failure when the tandem would be placed at the critical position for flexure (4.63 m from support 1 for span 1 and 5.50 m from support 2 for span 2).

8. Summary and Conclusions

The ageing bridge stock in the Netherlands has led to research on reinforced concrete slab bridges, as well as research on load testing for cases of bridges with material deterioration or when doubts about the structural system arise. In the Netherlands, there are especially concerns about the shear capacity of the existing reinforced concrete slab bridges, because initial assessments showed high Unity Checks for the existing reinforced concrete slab bridges. Moreover, shear is a brittle failure mode, which is an additional cause for concerns.

For the Ruytenschildt bridge, a load test was carried out, and then the load was further increased to achieve failure. Two spans of this bridge were tested in August 2014. The Ruytenschildt Bridge, opened in 1962, could be tested to failure since it was being replaced for functional reasons. This bridge has a skew angle of 18^{o}. The material parameters were determined from samples from the bridge.

During the testing of the Ruytenschildt Bridge, a load spreader system was used to avoid major damage at collapse. The loading position was chosen as the critical

loading position for shear, to study the most unfavourable loading situation for shear. It was found in the experiments that failure only could be achieved in span 2. Flexural failure with a support settlement occurred in span 2. The maximum load was in between the axle load corresponding with the predicted yield and ultimate moment, so good correspondence with the test results was obtained for flexure.

To further analyse the safety of the bridge, the current rating procedures, and the bending moment capacity of the Ruytenschildt Bridge, a study based on a linear elastic finite element model of the bridge was executed. The proof load level for flexure was determined, and it was concluded that the bridge would have been approved as having sufficient capacity in a proof load test. A finer plastic analysis was carried out, assuming a plastic hinge at the yielded parts in a beam model. This beam model did not allow for further plastic redistribution after the development of the first plastic hinge. A sharper study based on the linear elastic finite element model studying the bridge as a slab and using the observed yield lines from the test was then carried out.

Finally, the Unity Checks for flexure for spans 1 and 2 were determined. These Unity Checks showed that the bridge would rate sufficient for flexure and that the tested cross-sections have a larger capacity than predicted. The rating procedures are thus conservative.

Notation List

The following symbols are used in this paper:

α_{qi} multiplication factors for live load model 1

β reliability index

β_1 parameter that determines average compressive stress in concrete

β_{ult} parameter that gives relation between height of rectangular compressive stress block and depth of the compression zone

ε_c strain in concrete fiber most in compression

ε_{ult} strain at crushing of the concrete

ε_0 material parameter of the concrete

ξ unknown

ρ_l longitudinal reinforcement ratio

b member width

b_{para} effective width based on a load spreading parallel to the straight case

b_{skew} effective width with horizontal load spreading under 45^o from the far side of the wheel print to the face of the support

b_{str} effective width for a straight slab

b_w web width

c_y depth of the compression zone at yielding of the tension steel

c_{ult} depth of the compression zone at the ultimate

d_l effective depth to the longitudinal reinforcement

d' distance between fiber most in compression and centroid of compression steel

f_{ck} characteristic cube compressive strength

f_{cm} average cube compressive strength

$f_{cm,cyl}$ average cylinder compressive strength

$f_{c,th}$ stress in the concrete using Thorenfeldt's stress-strain diagram at yielding of the steel

f_r modulus of rupture of concrete

f_s' compressive stress in the compression steel at the ultimate

f_u average ultimate strength of steel

f_y average yield strength

f_{yk} characteristic yield strength

k size effect factor

k_2 factor for the centroid of the concrete compressive stress distribution

k_{th} parameter related to Thorenfeldt's stress-strain diagram, indicating the relative position to the peak of the diagram

m_{ux}^+ combined longitudinal moment

m_{uy}^+ combined transverse moment

m_x longitudinal bending moment

m_{xy} torsional moment

m_y transverse bending moment

m_{yield} yield moment in kNm/m

n_{th} material parameter of concrete

v_{min} lower bound of the shear capacity

x position of x-coordinate of face of the tandem

$y_{tension}$ distance between neutral axis and tension face

A_s area of steel

$A_{s,comp}$ area of compression steel

C_c resultant of concrete in compression

C_s resultant of steel in compression

$C_{R,c}$ calibration factor for the average value of the shear capacity

E_c Young's modulus of concrete

EW east-west direction, longitudinal direction

I_g moment of inertia of the gross (uncracked) section

$LEpart$ linear elastic part of moment

$LEpart_{max}$ increased moment to achieve the yield moment of the cross-section

NS north-south direction, transverse direction

M_{cr} moment causing cracking of the cross-section

$M_{plastic}$ yield moment multiplied with crack length

M_{test} maximum moment in cross-section at experiment

M_u moment causing crushing of the concrete in the cross-section

M_y moment causing yielding of the steel in the cross-section

P_{cr} tandem load corresponding to moment causing cracking of the cross-section

P_{tot} expected maximum tandem load for shear failure

$P_{tot,slab}$ expected maximum tandem load for shear failure taking into account the magnification factor for the shear capacity of slabs

P_u tandem load corresponding to moment at the ultimate

P_y tandem load corresponding to moment at yielding

$V_{R,c}$ average value of the shear capacity

Acknowledgement

The authors wish to express their gratitude and sincere appreciation to the Province of Friesland and the Dutch Ministry of Infrastructure and the Environment (Rijkswaterstaat) for financing this research work. The contributions and help of our colleagues A. Bosman, S. Fennis, P. van Hemert and Y. Yang, of the contractor de Boer en de Groot, and of Mammoet, responsible for applying the load, are gratefully acknowledged.

References

ACI Committee 437. (2013). *Code Requirements for Load Testing of Existing Concrete Structures (ACI 437.2M-13) and Commentary* Farmington Hills, MA, 24 pp.

Aktan, A. E., Zwick, M., Miller, R., & Shahrooz, B. (1992). Nondestructive and Destructive Testing of Decommissioned Reinforced Concrete Slab Highway Bridge and Associated Analytical Studies. *Transportation Research Record: Journal of the Transportation Research Board, 1371*, 142-153.

Allbright, K., Parekh, K., Miller, R. and Baseheart, T. M., 1995, "Modal verification of a destructive test of a damaged prestressed concrete beam," *Experimental Mechanics*, 34(4), 389-396.

Anay, R., Cortez, T. M., Jáuregui, D. V., El Batanouny, M. K. and Ziehl, P., 2016, "On-Site Acoustic-Emission Monitoring for Assessment of a Prestressed Concrete Double-Tee-Beam Bridge without Plans," *Journal of Performance of Constructed Facilities*, (available online ahead of print).

Azizinamini, A., Boothby, T. E., Shekar, Y., & Barnhill, G. (1994). Old Concrete Slab Bridges. 1. Experimental Investigation. *Journal of Structural Engineering-Asce, 120*(11), 3284-3304.

Azizinamini, A., Shekar, Y., Boothby, T. E., & Barnhill, G. (1994). Old concrete slab bridges. 2: Analysis. *Journal of Structural Engineering-Asce, 120*(11), 3305-3319.

Bagge, N., Sas, G., Nilimaa, J., Blanksvard, T., Elfgren, L., Tu, Y., & Carolin, A. (2015). *Loading to failure of a 55 year old prestressed concrete bridge*. Paper presented at the IABSE Workshop, Helsinki, Finland.

Bagge, N., Shu, J., Plos, M., & Elfgren, L. (2015). *Punching Capacity of a Reinforced Concrete Bridge Deck Slab Loaded to Failure*. Paper presented at the IABSE 2015.

Bakht, B. and Jaeger, L. G., 1992, "Ultimate Load Test of Slab-on-Girder Bridge," *Journal of Structural Engineering*, 118(6), 1608-1624.

Bergström, M., Täljsten, B. and Carolin, A., 2009, "Failure Load Test of a CFRP Strengthened Railway Bridge in Örnsköldsvik, Sweden," *Journal of Bridge Engineering*, 14(5), 300-308.

Brühwiler, E., Vogel, T., Lang, T., & Luechinger, P. (2012). Swiss Standards for Existing Structures. *Structural Engineering International, 22*(2), 275-280. doi:10.2749/101686612x13291382991209

Cai, C. S., & Shahawy, M. (2003). Understanding Capacity Rating of Bridges from Load Tests. *Practice Periodical on Structural Design and Construction, 8*, 209-2016.

Casas, J. R., & Gómez, J. D. (2013). Load Rating of Highway Bridges by Proof-loading. *KSCE Journal of Civil Engineering, 17*(3), 556-567.

CEN. (2003). Eurocode 1: Actions on structures - Part 2: Traffic loads on bridges, NEN-EN 1991-2:2003 (pp. 168). Brussels, Belgium: Comité Européen de Normalisation.

CEN. (2005). Eurocode 2: Design of Concrete Structures - Part 1-1 General Rules and Rules for Buildings. NEN-EN 1992-1-1:2005 (pp. 229). Brussels, Belgium: Comité Européen de Normalisation.

Cochet, D., Corfdir, P., Delfosse, G., Jaffre, Y., Kretz, T., Lacoste, G., . . . Prat, M. (2004). *Load tests on highway bridges and pedestrian bridges (in French)*. Bagneux-Cedex, France.

Code Committee 351001. (2011). *Assessement of structural safety of an existing structure at repair or unfit for use - Basic Requirements, NEN 8700:2011 (in Dutch)*. Delft, The Netherlands: Civil center for the execution of research and standard, Dutch Normalisation Institute.

Cope, R. J. (1985). Flexural Shear Failure of Reinforced-Concrete Slab Bridges. *Proceedings of the Institution of Civil Engineers Part 2-Research and Theory, 79*(SEP), 559-583.

Cope, R. J., & Rao, P. V. (1983). Moment Redistribution in Skewed Slab Bridges. *Proceedings of the Institution of Civil Engineers Part 2-Research and Theory, 75*(SEP), 419-451.

Cope, R. J., Rao, P. V., & Edwards, K. R. (1983). *Shear in skew reinforced concrete slab bridges – analytical and experimental studies – A report to the Department of Transport*. Liverpool, UK-

Cullington, D. W., Daly, A. F., & Hill, M. E. (1996). Assessment of reinforced concrete bridges: Collapse tests on Thurloxton underpass. *Bridge Management, 3*, 667-674.

Cusens, A. R. (1987). Free edge and obutse corner shear in R/C skew bridge decks. *ACI Structural Journal, 84*(6), 537-537.

Deutscher Ausschuss für Stahlbeton. (2000). *DAfStb-Richtlinie: Belastungsversuche an Betonbauwerken*. Deutscher Ausschuss fur Stahlbeton,, 7 pp.

Farhey, D. N. (2005). Bridge Instrumentation and Monitoring for Structural Diagnostics. *Structural Health Monitoring, 4*(4), 301-318.

Fennis, S., van Hemert, P., Hordijk, D., & de Boer, A. (2014). Proof loading Vlijmen-Oost; Research on assessment method for existing structures. *Cement, 5*, 40-45. (in Dutch)

Fennis, S. A. A. M., & Hordijk, D. A. (2014). *Proefbelasting Halvemaansbrug Alkmaar*. Stevin Report 25.5-14-05, Delft, The Netherlands.

Haritos, N., Hira, A., Mendis, P., Heywood, R., & Giufre, A. (2000). Load testing to collapse limit state of Barr Creek Bridge. *Transportation Research Record*(1696), A92-A102.

Jauregui, D. V., Licon-Lozano, A., & Kulkarni, K. (2010). Higher Level Evaluation of a Reinforced Concrete Slab Bridge. *Journal of Bridge Engineering, 15*(2), 172-182. doi:10.1061/(asce)be.1943-5592.0000047

Jiaquan, X., Zanping, W., Bing, H., Guanhua, F., Yufeng, Z. and Jianfei, Z., 2006, "Practical experimental study on ultimate bearing capacity of actual bridge in Huning Expressway Extension project," *Modern Transportation Technology*, 5, 77-84.

Jorgenson, J. L., & Larson, W. (1976). Field Testing of a Reinforced Concrete Highway Bridge to Collapse. *Transportation Research Record: Journal of the Transportation Research Board, 607*, 66-71.

Koekkoek, R., Lantsoght, E. O. L., Yang, Y., De Boer, A., & Hordijk, D. (2016). *Defining loading criteria for proof loading of existing reinforced concrete bridges*. Paper presented at the Performkance-based approaced for concrete structures, Cape Town, South Africa.

Koekkoek, R. T., Lantsoght, E. O. L., & Hordijk, D. A. (2015). *Proof loading of the ASR-affected viaduct Zijlweg over highway A59*. Stevin Report 25.5-15-08. Delft, The Netherlands.

Koekkoek, R. T., Lantsoght, E. O. L., Yang, Y., & Hordijk, D. A. (2016). *Analysis report for the assessment of Viaduct De Beek by Proof Loading*. Stevin Report 25.5-16-01. Delft, The Netherlands.

Koekkoek, R. T., Yang, Y., Fennis, S. A. A. M., & Hordijk, D. A. (2015). *Assessment of Viaduct Vlijmen Oost by Proof Loading*. Stevin Report 25.5-15-10. Delft, the Netherlands.

König, G. and Fischer, J., 1995, "Model Uncertainties concerning Design Equations for the Shear Capacity of Concrete Members without Shear Reinforcement," *CEB Bulletin 224, Model Uncertainties and Concrete Barrier for Environmental Protection*, 49-100.

Lantsoght, E. O. L. (2012). *Progress report: experiments on slabs in reinforced concrete. Part II: analysis of results (in Dutch)*. Stevin Report 25.5-12-10, Delft University of Technology, The Netherlands

Lantsoght, E. O. L., 2013. "Shear in Reinforced Concrete Slabs under Concentrated Loads Close to Supports," Ph.D. Thesis, Delft University of Technology, Delft, pp. 343.

Lantsoght, E. O. L. (2015). *Ruytenschildt Bridge: analysis of test results at the ultimate limit state (in Dutch)*. Stevin Report Nr. 25.5-15-05, Delft University of Technology, Delft, The Netherlands

Lantsoght, E. O. L., De Boer, A., & van der Veen, C. (2014). *Determination of distribution width for shear stresses at support in reinforced concrete slab bridges*. Paper presented at the EuroC, St. Anton am Arlberg, Austria.

Lantsoght, E. O. L., de Boer, A., van der Veen, C., & Walraven, J. (2015). Effective shear width of concrete slab bridges. *Proceedings of the Institution of Civil Engineers – Bridge Engineering, 168*(BE4), 287-298.

Lantsoght, E. O. L., de Boer, A., Van der Veen, C., & Walraven, J. C. (2013). *Peak shear stress distribution in finite element models of concrete slabs*. Paper presented at the Research and Applications in Structural Engineering, Mechanics and Computation, Cape Town, South Africa.

Lantsoght, E. O. L., van der Veen, C., De Boer, A., & Walraven, J. (2014). Influence of Width on Shear Capacity of Reinforced Concrete Members. *Aci Structural Journal, 111*(6), 1441-1450.

Lantsoght, E. O. L., van der Veen, C., de Boer, A., & Walraven, J. (in press). Transverse Load Redistribution and Effective Shear Width in Reinforced Concrete Slabs. *Heron*, 29 pp. .

Lantsoght, E. O. L., van der Veen, C., de Boer, A., & Walraven, J. C. (2013). Recommendations for the Shear Assessment of Reinforced Concrete Slab Bridges from Experiments *Structural Engineering International, 23*(4), 418-426.

Lantsoght, E. O. L., van der Veen, C., & Walraven, J. C. (2013). Shear in One-way Slabs under a Concentrated Load close to the support. *ACI Structural Journal, 110*(2), 275-284.

Lantsoght, E. O. L., van der Veen, C., Walraven, J. C., & de Boer, A. (2016). Case Study on Aggregate Interlock Capacity for the Shear Assessment of Cracked Reinforced-Concrete Bridge Cross Sections. *Journal of Bridge Engineering, 21*(5), 04016004-04016001-04016010. doi:10.1061/(ASCE)BE.1943-5592.0000847

Menassa, C., Mabsout, M., Tarhini, K., & Frederick, G. (2007). Influence of skew angle on reinforced concrete slab bridges. *Journal of Bridge Engineering, 12*(2), 205-214. doi:10.1061/(asce)1084-0702(2007)12:2(205)

Miller, R. A., Aktan, A. E., & Shahrooz, B. M. (1994). Destructive testing of decommisisioned concrete slab bridge. *Journal of Structural Engineering-Asce, 120*(7), 2176-2198.

Moses, F., Lebet, J. P., & Bez, R. (1994). Applications of field testing to bridge evaluation. *Journal of Structural Engineering-Asce, 120*(6), 1745-1762. doi:10.1061/(asce)0733-9445(1994)120:6(1745)

NCHRP. (1998). *Manual for Bridge Rating through Load Testing*. Washington, DC.

Nemetschek Scia. (2016). *Scia helpfile release 15.2*.
NRA. (2014). *Load Testing for Bridge Assessment*. Dublin, Ireland.
Olaszek, P., Świt, G. and Casas, J. R., (2012), "Proof load testing supported by acoustic emission - an example of application", *IABMAS 2012*.
Olaszek, P., Lagoda, M., & Ramon Casas, J. (2014). Diagnostic load testing and assessment of existing bridges: examples of application. *Structure and Infrastructure Engineering, 10*(6), 834-842. doi:10.1080/15732479.2013.772212
Pape, T. M. and Melchers, R. E. (2010) "The effects of corrosion on 45-year-old pre-stressed concrete bridge beams," *Structure and Infrastructure Engineering*, 7(1-2), 101-108.
Puurula, A. M., Enochsson, O., Sas, G., Blanksvärd, T., Ohlsson, U., Bernspång, L., Täljsten, B. and Elfgren, L., (2014), "Loading to failure and 3D nonlinear FE modelling of a strengthened RC bridge," *Structure and Infrastructure Engineering*, 10(12), 1606-1619.
Puurula, A. M., Enochsson, O., Sas, G., Blanksvärd, T., Ohlsson, U., Bernspång, L., Täljsten, B., Carolin, A., Paulsson, B. and Elfgren, L., (2015) "Assessment of the Strengthening of an RC Railway Bridge with CFRP Utilizing a Full-Scale Failure Test and Finite-Element Analysis," *Journal of Structural Engineering*, 141(1), D4014008.
Rijkswaterstaat. (2013a). *Assumptions QS Slabs 2012 - skew factors 2012*.
Rijkswaterstaat. (2013b). Guidelines Assessment Bridges - assessment of structural safety of an existing bridge at reconstruction, usage and disapproval (in Dutch) (pp. 117).
Rogers, R. A., Wotherspoon, L., Scott, A. and Ingham, J. M., 2012, "Residual strength assessment and destructive testing of decommissioned concrete bridge beams with corroded pretensioned reinforcement," *PCI Journal*, 57(3), 100-118.
Roschke, P. N. and Pruski, K. R., 2000, "Overload and Ultimate Load Behavior of Posttensioned Slab Bridge," *Journal of Bridge Engineering*, 5(2), 148-155.
Russo, F. M., Wipf, T. J., & Klaiber, F. W. (2000). Diagnostic Load Tests of a Prestressed Concrete Bridge Damaged by Overheight Vehicle Impact. *Transportation Research Record, 1696*, 103-110.
Saraf, V., Sokolik, A. F., & Nowak, A. S. (1996). Proof Load Testing of Highway Bridges. *Transportation Research Record, 1541*, 51-57.
Schacht, G., Bolle, G., Curbach, M., & Marx, S. (2016). Experimental Evaluation of the shear bearing safety. *Beton- und Stahlbetonbau, 111*(6), 343-354.
Siringoringo, D. M., Fujino, Y. and Nagayama, T., 2013, "Dynamic Characteristics of an Overpass Bridge in a Full-Scale Destructive Test," *Journal of Engineering Mechanics-ASCE*, 139(6), 691-701.
Stichting Commissie Voorschriften Beton. (1977). *Provisions Concrete VB 1977 - Part E: Reinforced Concrete, additional provisions (NEN 3865) (in Dutch)*. Delft, the Netherlands.
Tersteeg, R. H. D., 2015, "Proof load testing of concrete bridges" B.Sc. Thesis, Delft University of Technology, Delft, The Netherlands, pp. 69. (in Dutch)
The Institution of Civil Engineers - National Steering Committee for the Load Testing of Bridges. (1998). *Guidelines for the Supplementary Load Testing of Bridges*. London, UK.
Theoret, P., Massicotte, B., & Conciatori, D. (2012). Analysis and Design of Straight and Skewed Slab Bridges. *Journal of Bridge Engineering, 17*(2), 289-301. doi:10.1061/(asce)be.1943-5592.0000249

Veneziano, D., Galeota, D., & Giammatteo, M. M. (1984). Analysis of bridge proof-load data I: Model and statistical procedures. *Structural Safety, 2*, 91-104.

Vergoossen, R., Naaktgeboren, M., ‘t Hart, M., De Boer, A., & Van Vugt, E. (2013). *Quick Scan on Shear in Existing Slab Type Viaducts*. Paper presented at the International IABSE Conference, Assessment, Upgrading and Refurbishment of Infrastructures, Rotterdam, The Netherlands.

Wang, F. M., Kang, S. Z., Cai, Y. C. and Li, X. L., 2011, "Destructive Test Study of A Prestressed Concrete Hollow Slab Beam Bridge," *Geotechnical Special Publication No. 214 - American Society of Civil Engineers*, 57-64.

Wood, R. H., 1968, "The reinforcement of slabs in accordance with a pre-determined field of moments," *Concrete*, February, 69-76.Yang, Y., 2015, "Experimental Studies on the Structural Behaviours of Beams from Ruytenschildt Bridge," *Stevin Report 25.5-15-09*, Delft University of Technology, Delft, 76 pp.

Yang, Y. and Hordijk, D. A., 2015, "Acoustic Emission Measurement and Analysis on Zijlwegbrug," Stevin Report Nr. 25.5-15-01, Delft University of Technology, Delft, The Netherlands, 27 pp.

Zhang, J.-r., Peng, H., Zhang, K.-b. and Hao, H.-x., 2009, "Test Study on Overload and Ultimate Behavior of Old Reinforced Concrete Bridge Through Destructive Test of Corroded Bridge," *Engineering Mechanics*, 26(12), 213-224.

Zhang, J., Peng, H. and Cai, C. S., 2011, "Field Study of Overload Behavior of an Existing Reinforced Concrete Bridge under Simulated Vehicle Loads," *Journal of Bridge Engineering*, 16(2), 226-237.

Zhang, J., Peng, H. and Cai, C. S., 2013, "Destructive Testing of a Decommissioned Reinforced Concrete Bridge," *Journal of Bridge Engineering*, 18(6), 564-569.

Ziemian, R. D., & McGuire, W. (2015). *MASTAN2 v3.5*.

List of Tables

Table 1. Overview of past testing to failure on bridges

Reference	Bridge name	Type of bridge	Failure mode
(Haritos, Hira, Mendis, Heywood, & Giufre, 2000)	Barr Creek	slab bridge	Flexural failure
(Azizinamini, Boothby, Shekar, & Barnhill, 1994; Azizinamini, Shekar, Boothby, & Barnhill, 1994)	Niobrara River	slab bridge	Flexural failure
(Aktan, Zwick, Miller, & Shahrooz, 1992; Miller, Aktan, & Shahrooz, 1994)	---	slab bridge	Punching failure
(Jorgenson & Larson, 1976)	ND-18	slab bridge	Flexural failure
(Bagge, Sas, et al., 2015; Bagge, Shu, Plos, & Elfgren, 2015)	Kiruna	prestressed girder bridge	Punching failure
(Wang et al. 2011)	East Meng Jiang Nu Bridge	prestressed hollow core slab bridge	Flexural failure
(Bergström et al. 2009; Elfgren 2011; Puruula et al. 2014, 2015)	Örnsköldsvik Bridge	through bridge	Shear failure*
(Zhang et al. 2011; Zhang et al. 2009; Zhang et al. 2013)	Nanping bridge	channel beam bridge	Flexural failure
(Bakht and Jaeger 1992)	Stony Creek Bridge	concrete deck on steel girders	Yielding of steel girder
(Jiaquan et al. 2006)	Huning Expressway Bridge	box girder bridge	Flexural failure

* The Örnsköldsvik Bridge was strengthened with CFRP reinforcement to avoid a bending failure and induce shear failure.

Table 2. Available reinforcement

	Span 1		Span 2	
Reinforcement	Support 1	Span 1	Support 2	Span 2
Longitudinal, bottom	ϕ19–270 ϕ22-270	ϕ19–270 2×ϕ22-270	ϕ19–270	ϕ16–270 2×ϕ22-270
Longitudinal, top	ϕ22-270 ϕ12-130	ϕ10-130 ϕ19–270	4×ϕ22-270	ϕ12-130 ϕ22-270

Table 3. Calculated shear and moment capacity of tested spans. P_{tot} is the total predicted maximum load, and $P_{tot,slab}$ is the increased load based on the magnification factor from experiments on straight slabs, with effective widths b_{str}, b_{para} and b_{skew} as shown in Figure 4. M_{cr} is the moment at cracking, M_y the moment at yielding and M_u the moment at the ultimate. The corresponding tandem loads are P_{cr}, P_y and P_u. The maximum moment in the experiment is M_{test}.

Span	Span 1		Span 2	
Shear capacity	P_{tot} [kN]	$P_{tot,slab}$ [kN]	P_{tot} [kN]	$P_{tot,slab}$ [kN]
b_{str}	3760	5512	4020	5893
b_{para}	3236	4744	3432	5031
b_{skew}	4804	7043	5328	7811
Experiment	≥ 3049		≥ 3991	
Flexural capacity	Span		Support	Span
P_{cr} (kN)	880		1432	1460
P_y (kN)	2368		7720	3532
P_u (kN)	3102		9940	4496
Flexural capacity	Span moment		Support moment	Span moment
M_{cr} (kNm)	1816		1690	1592
M_y (kNm)	3925		5662	3717
M_u (kNm)	4964		7064	4705
M_{test} (kNm)	4889		3306	4188

Table 4. Calculated moments at position x causing largest moment with the Eurocode loads, and calculated moments for maximum load on proof load tandem. m_x is the bending moment, m_{xy} the torsional moment and m_{ux}^+ the moment based on Wood and Armer's combination of bending and torsional moments (Wood, 1968).

	EC load		Proof load	
	Span 1	Span 2	Span 1	Span 2
x (m)	4.63	14.50	3.39	12.46
m_x (kNm/m)	417.87	325.16	803.26	810.08
m_{xy} (kNm/m)	-20.62	-5.28	-16.36	-4.19
m_{ux}^+ (kNm/m)	438.49	330.44	819.62	814.27

Table 5. Observed cracks (see Figure 11) and determined yield moments m_{yield} as the yield moment for the provided reinforcement per unit length, and $M_{plastic}$ the total yield moment of the crack, i.e. the product of the length and $m_{yield.}$

Nr.	Direction	Length [m]	m_{yield} [kNm/m]	$M_{plastic}$ [kNm]
1	EW	3.47	504.6	1832
2	NS	2.35	95.5	224
3	NS	3.63	95.5	331

Table 6. Overview of calculated loads and capacities, and resulting Unity Checks. The presented values are recalculated axle loads to achieve the same result, given in [kN].

Load				Capacity				
Equivalent		In test		Moment capacity		Mechanism		
Span 1	Span 2	Span 1	Span 2	Span 1	Span 2	Span 1	Span 2	Refine Span 2
1240	1088	3049	3991	2368	3532	2368	3532	2376

Unity Check		Unity Check with proof load	
Span 1	Span 2	Span 1	Span 2
0.524	0.458	1.288	1.680

List of Figures

Figure 1. Photograph of Ruytenschildt bridge.

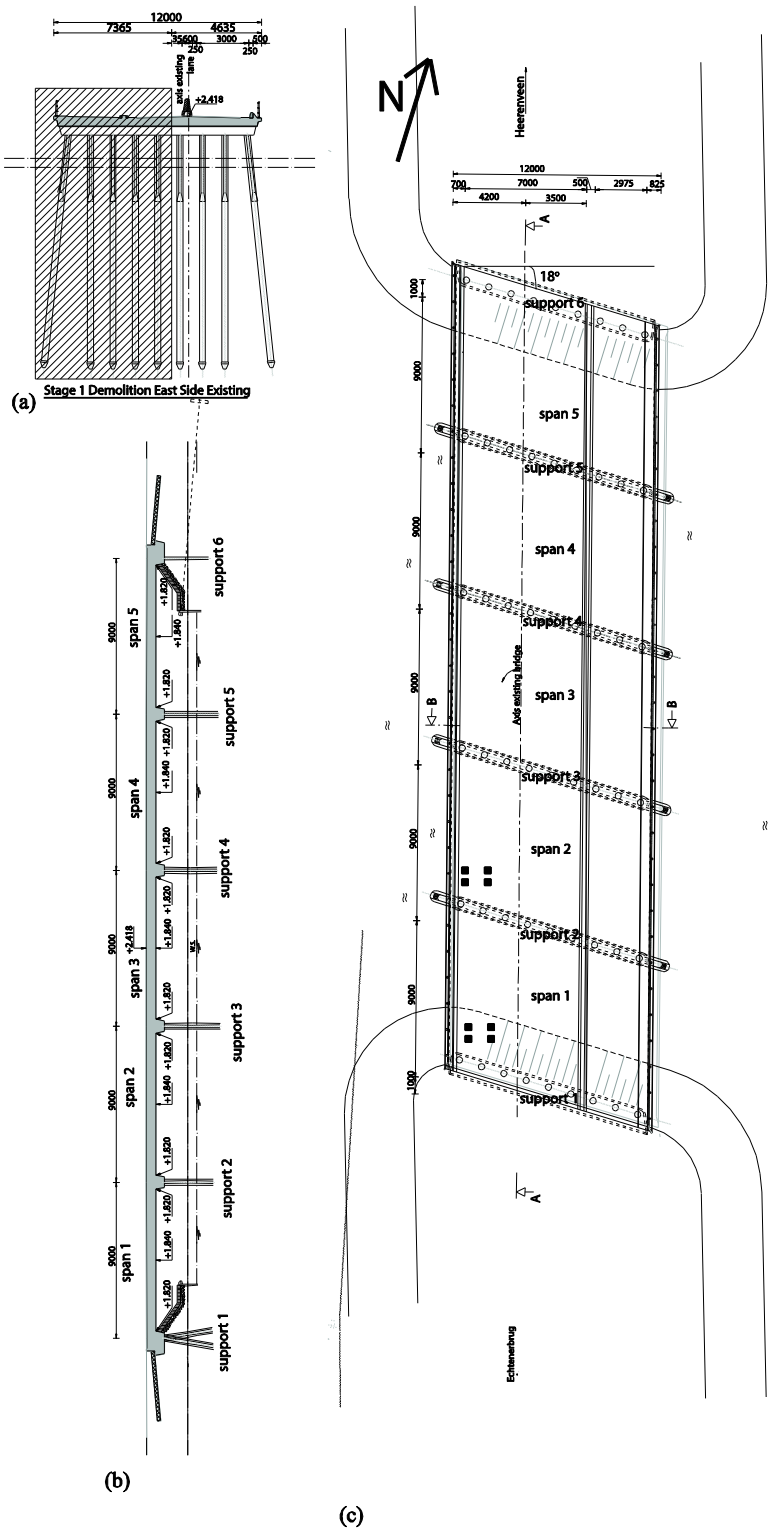

Figure 2. Overview of geometry of Ruytenschildt Bridge: (a) Cross-section showing the stages of demolition. The hatched area was tested to failure; (b) Side view; (c) Top view. Units: [mm].

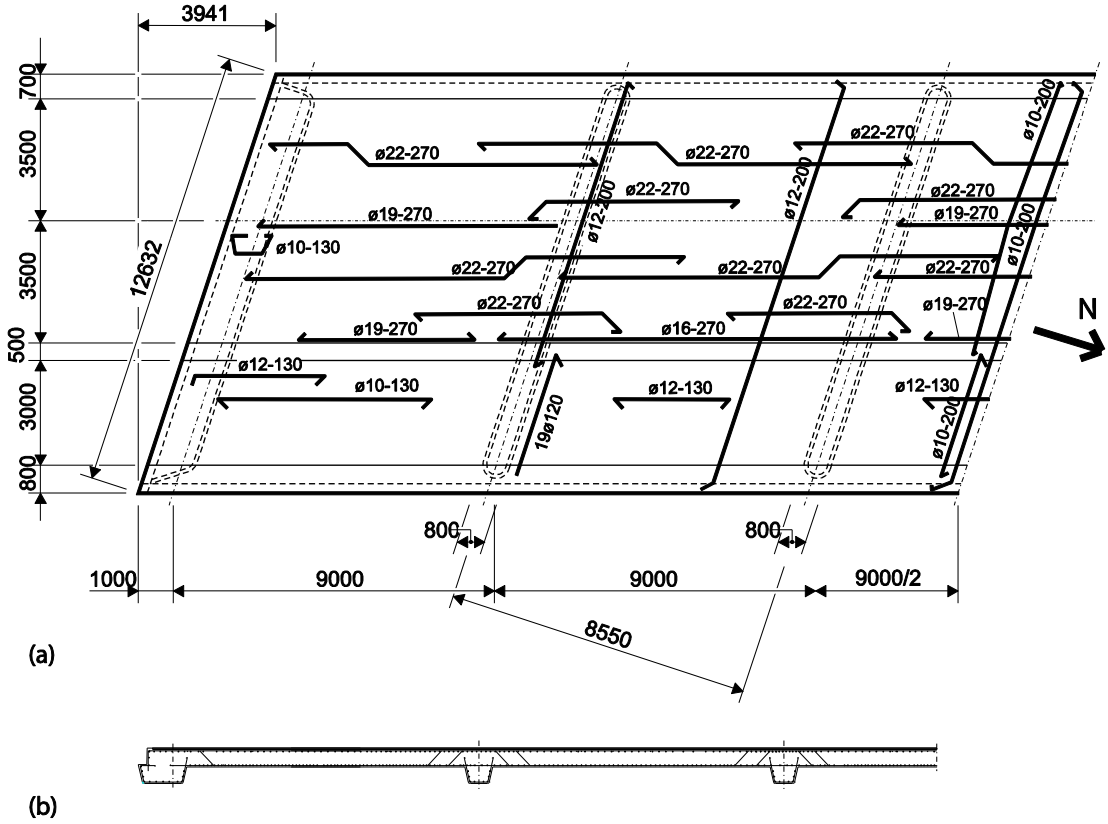

Figure 3. Reinforcement drawing of Ruytenschildt Bridge, showing spans 1, 2 and half of span 3: (a) Plan view; (b) cross-section. The structure is symmetric. Units: [mm].

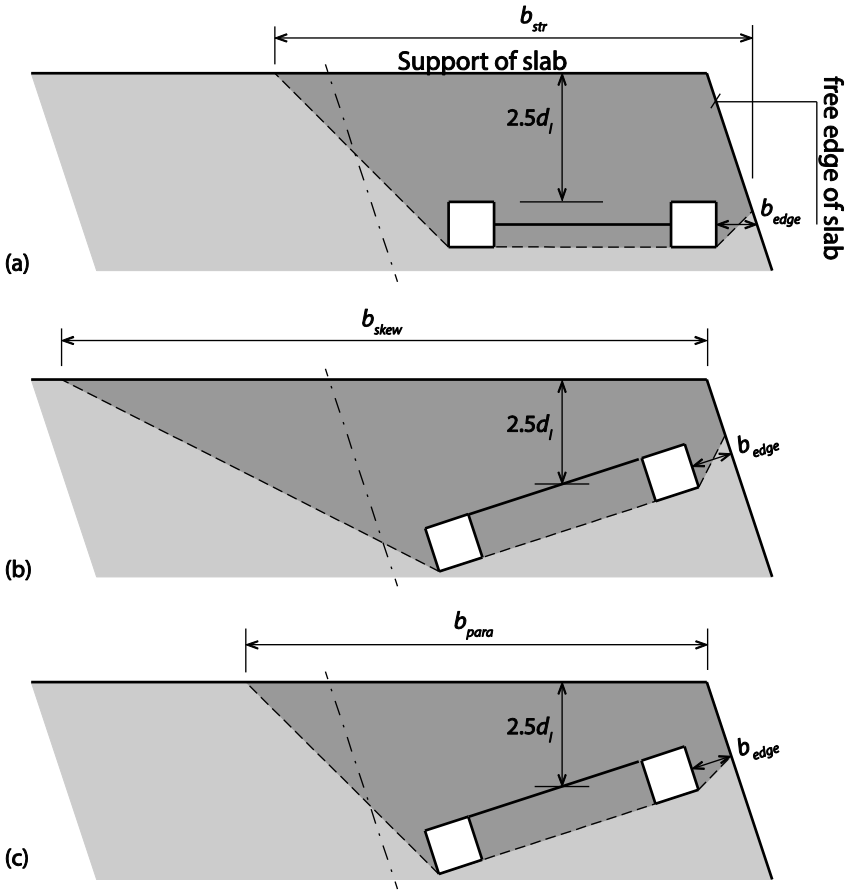

Figure 4. Top view of the slab showing first axle, support line and the free edge to explain the different possible interpretations for the effective widths for a skewed slab: (a) b_{str}, the effective width as for a straight slab; (b) b_{skew} the effective width with a horizontal load spreading under 45^{o} from the far side of the wheel print to the face of the support; and (c) b_{para} the effective width based on a load spreading parallel to the straight case.

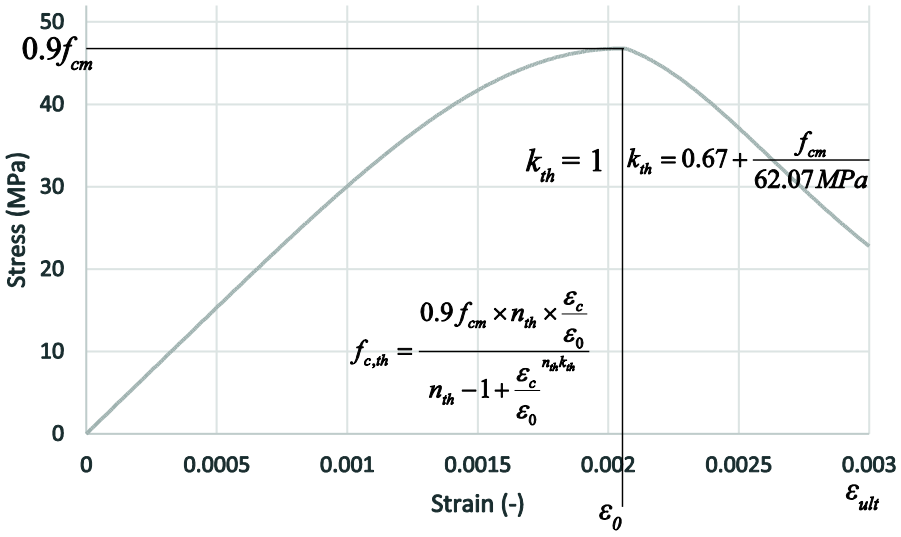

Figure 5. Thorenfeldt's stress-strain diagram, applied to f_{cm} = 52 MPa.

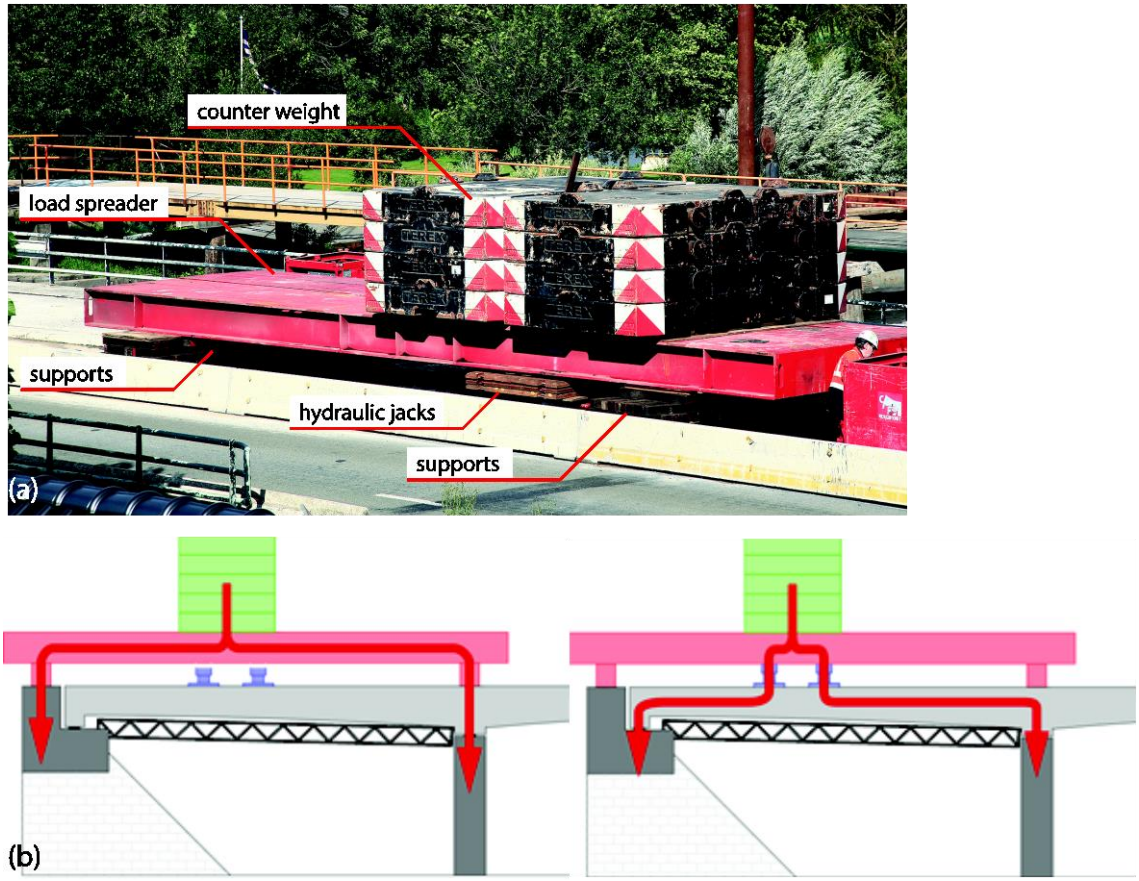

Figure 6. Load spreader system for loading the Ruytenschildt Bridge: (a) Photograph; (b) principle of unloaded and loaded situation

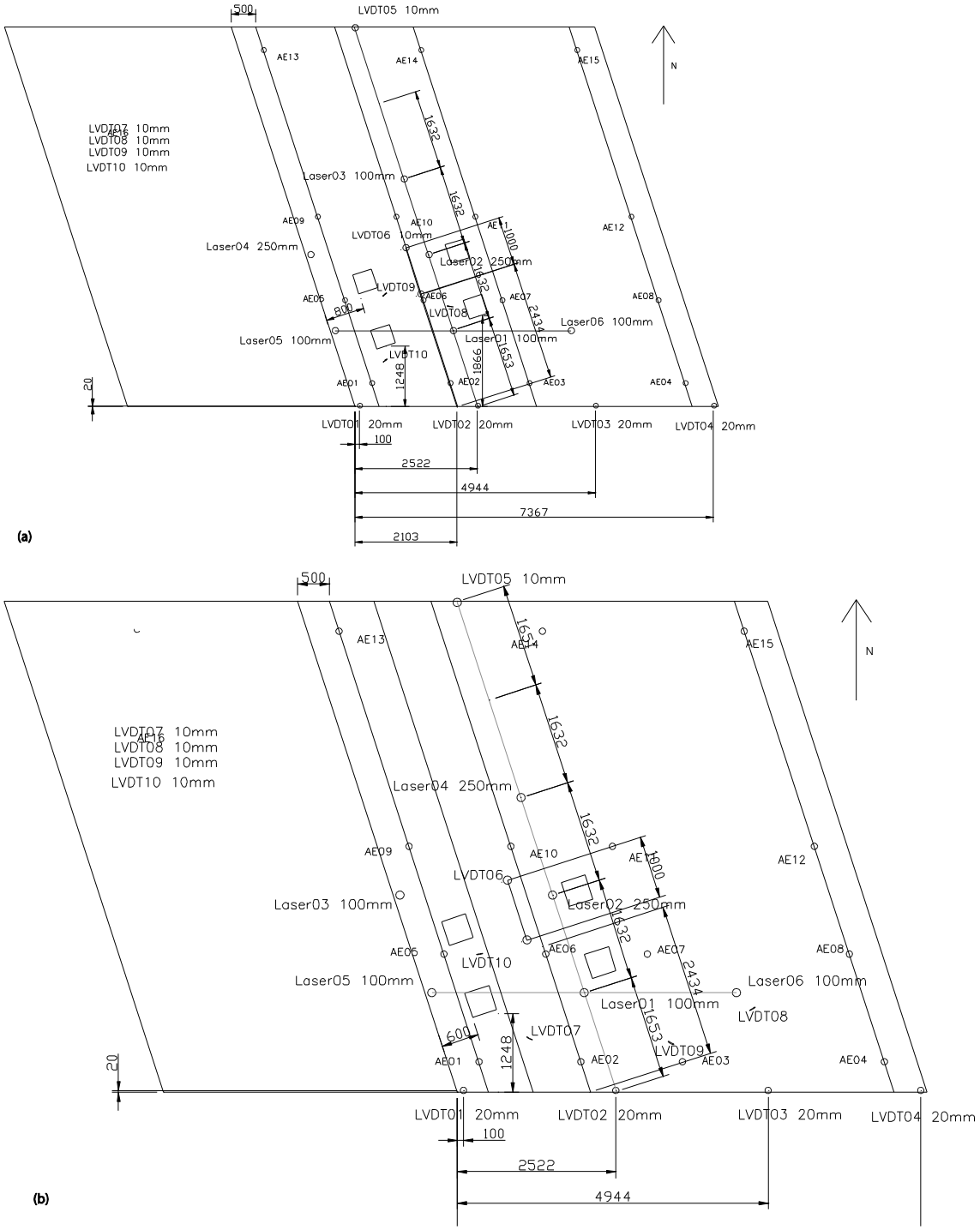

Figure 7. Sensor plan and position of wheel prints: (a) span 1, (b) span 2. Ranges of the sensors are given, and distances have units [mm].

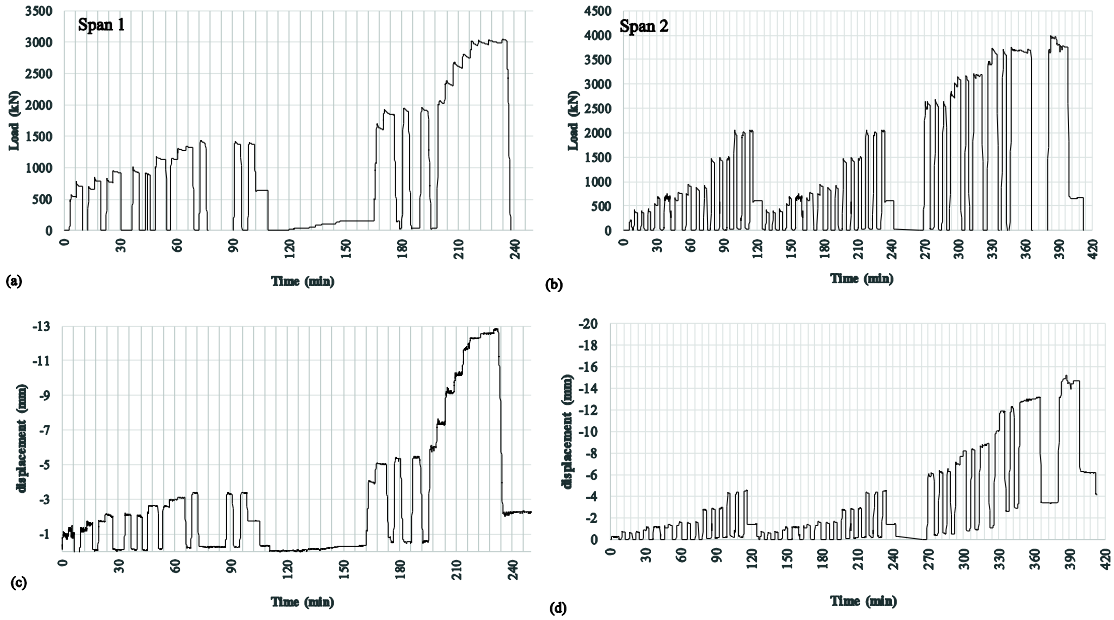

Figure 8. Loading diagram and displacement measurements of the Ruytenschildt Bridge: (a) Span 1, force versus time; (b) Span 2, force versus time; (c) Span 1, displacement measured by laser 1 versus time; (d) Span 2, displacement measured by laser 3 versus time.

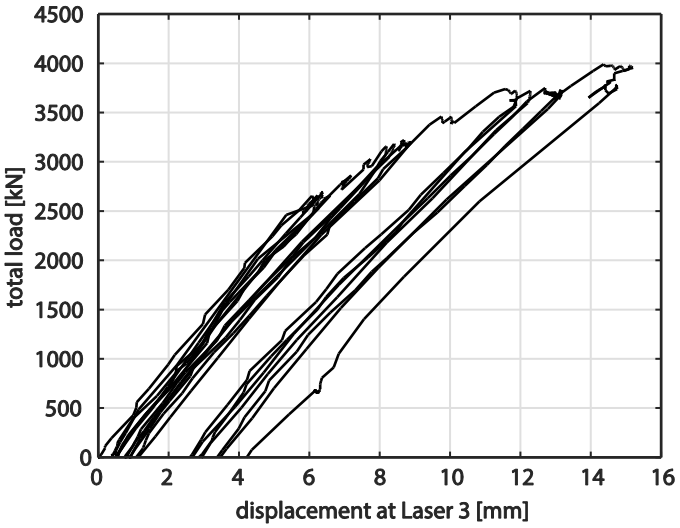

Figure 9. Load-displacement diagram of the test in Span 2.

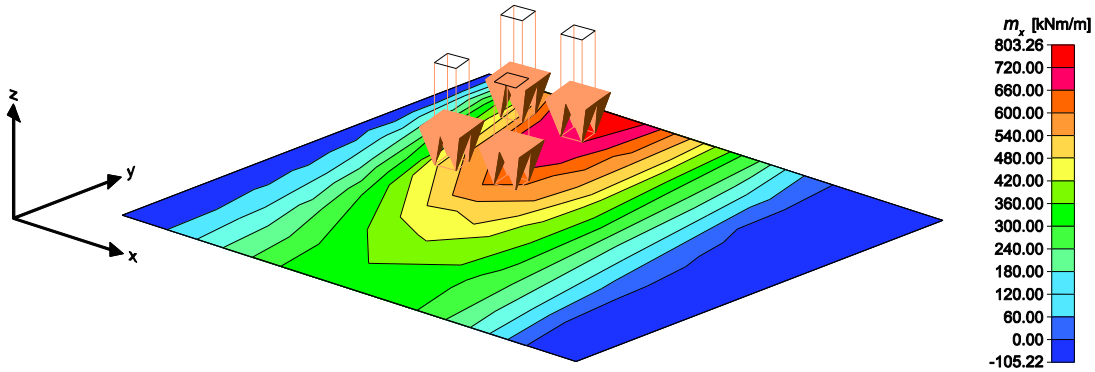

Figure 10. Results of finite element model for bending moment in the longitudinal direction m_x with maximum load in the experiment in Span 1

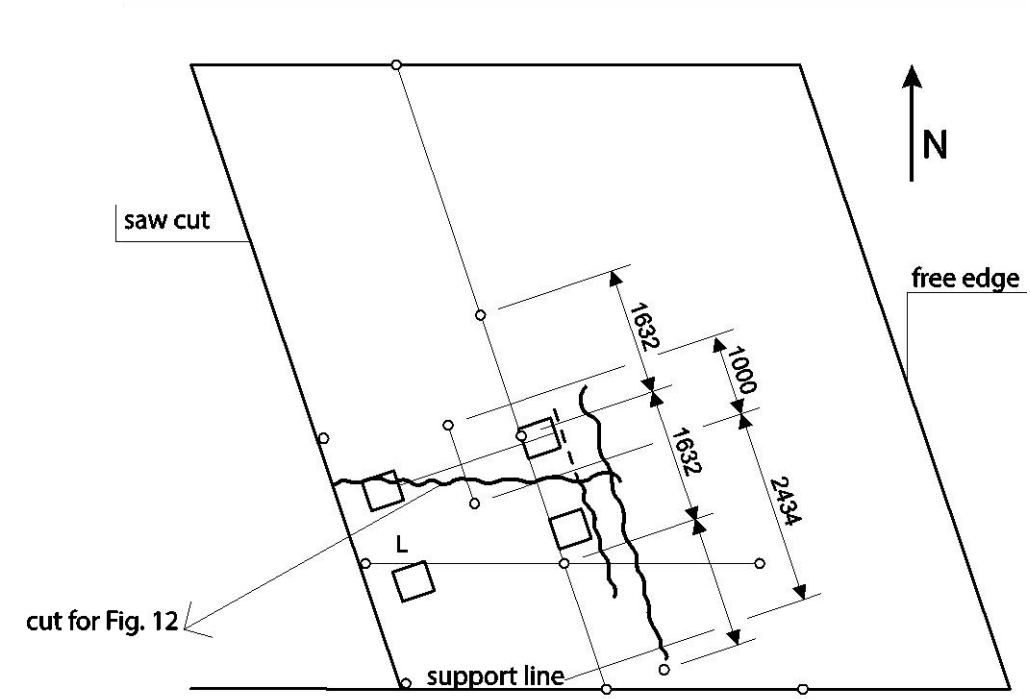

(a)

(b)

Figure 11. Cracks in Span 2 after experiment, bottom side of bridge deck: (a) sketch of cracks; (b) damage to the pier; (c) photograph of cracks on bottom of bridge slab

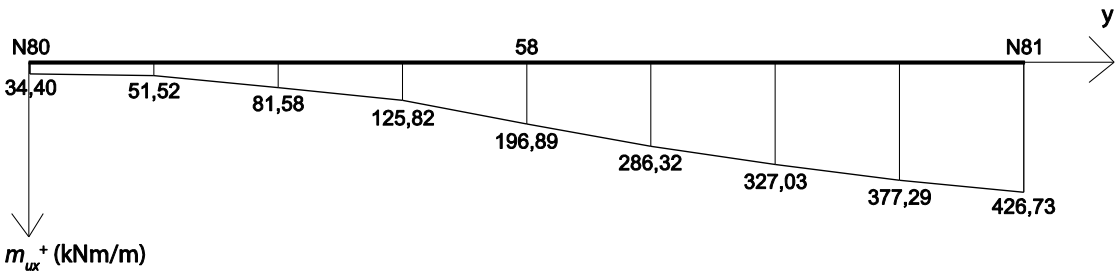

Figure 12. Moment diagram in *y*-direction at the location of the studied crack.